



HAL
open science

Pertinent parameters in photo-generation of electrons: Comparative study of anatase-based nano-TiO₂ suspensions

D Martel, A Guerra, P Turek, J Weiss, B Vilenó

► **To cite this version:**

D Martel, A Guerra, P Turek, J Weiss, B Vilenó. Pertinent parameters in photo-generation of electrons: Comparative study of anatase-based nano-TiO₂ suspensions. *Journal of Colloid and Interface Science*, 2016. hal-03810226

HAL Id: hal-03810226

<https://hal-cnrs.archives-ouvertes.fr/hal-03810226>

Submitted on 11 Oct 2022

HAL is a multi-disciplinary open access archive for the deposit and dissemination of scientific research documents, whether they are published or not. The documents may come from teaching and research institutions in France or abroad, or from public or private research centers.

L'archive ouverte pluridisciplinaire **HAL**, est destinée au dépôt et à la diffusion de documents scientifiques de niveau recherche, publiés ou non, émanant des établissements d'enseignement et de recherche français ou étrangers, des laboratoires publics ou privés.

Pertinent parameters in photo-generation of electrons: Comparative study of anatase-based nano-TiO₂ suspensions

D. Martel^{a,*}, A. Guerra^{a,b}, P. Turek^{b,d}, J. Weiss^c, B. Vilen^{b,d,*}

^a Centre National de la Recherche Scientifique, UPR 22, Institut Charles Sadron, 23 rue du loess, BP 84047, 67034 Strasbourg cedex 2, France

^b Propriétés Optiques et Magnétiques des Architectures Moléculaires (POMAM), Institut de Chimie, UMR 7177 CNRS/Université de Strasbourg, 4 rue Blaise Pascal, 67000 Strasbourg, France

^c Chimie des Ligands à Architecture Contrôlée (CLAC), Institut de Chimie, UMR 7177 CNRS/Université de Strasbourg, 1 rue Blaise Pascal, 67000 Strasbourg, France

^d French EPR Federation of Research (REseau NAional de Rpe interDisciplinaire (RENARD), Fédération IR-RPE CNRS #3443), France

Abstract

In the field of solar fuel cells, the development of efficient photo-converting semiconductors remains a major challenge. A rational analysis of experimental photocatalytic results obtained with material in colloidal suspensions is needed to access fundamental knowledge required to improve the design and properties of new materials. In this study, a simple system electron donor/nano-TiO₂ is considered and examined via spin scavenging electron paramagnetic resonance as well as a panel of analytical techniques (composition, optical spectroscopy and dynamic light scattering) for selected type of nano-TiO₂. Independent variables (pH, electron donor concentration and TiO₂ amount) have been varied and interdependent variables (aggregate size, aggregate surface vs. volume and acid/base groups distribution) are discussed. This work shows that reliable understanding involves thoughtful combination of interdependent parameters, whereas the specific surface area seems not a pertinent parameter. The conclusion emphasizes the difficulty to identify the key features of the mechanisms governing photocatalytic properties in nano-TiO₂.

Introduction

Since the beginning of mankind, the sun is the most abundant source of energy. Throughout centuries, attempts have been made to benefit from this free, and sustainable and renewable energy. In 1839, Becquerel discovered the photovoltaic effect allowing new route for solar

energy conversion. However, both the high cost of solar energy conversion devices and the parallel massive exploitation of fossil fuel in the middle of the 20th century hampered the development of this field. As a consequence of successive breakdown events such as the oil crisis in the 70s, the public belief has accepted the concept of limited fossil resources. Since then, the continuous increase of energy needs and the more recent problem of global warming have brought solar energy to the scientific societal and economical forefront. In this context, numerous studies about the photoactivity of different oxide semiconductors have been performed since the second half of last century [1]. In 1972, Fujishima and Honda [2] reported the photoactivity of the titanium oxide (TiO_2) for the water photolysis process: an important pathway in the research field of clean, sustainable and renewable energy production. Today silicon technology is the main actor in the photovoltaic devices. In comparison, the TiO_2 semiconductor has the advantage of being cheaper, while displaying good stability in solution towards photocorrosion [3]. In addition to its great intrinsic properties TiO_2 is yet one of the most studied semiconductor in the field of solar energy and for many others applications ranging from water and air purification to self-cleaning surfaces [1]. Abundant scientific reports have been focused on the photophysicochemical properties of TiO_2 , aiming at the rationalization of the semiconductor properties to optimize the performances of the material itself. Properties such as charge transfer, charge trapping, doping [4], loading [5] or surface states have been investigated by varying parameters such as the scale of material (bulk or nanosized) and the crystallographic structure (anatase, rutile and brookite). In the case of nanostructured TiO_2 , the size, shape (nanoparticle, nanorods, nanofibers [6]) and their specific surface area are currently under scrutiny. Despite the profusion of studies, a clear understanding of key parameters is not yet available. For instance, the photo-catalytic activity of the anatase phase compared to the rutile one is still debated [7]. In parallel, the photo catalytic efficiency of mixed phase rutile-anatase (e.g. commercial nano- TiO_2 P25 from DegussaTM) may be assigned to possible synergistic effects whereas other investigations conclude to the lack of particular features [8]. The complexity of theoretical modelling is further complicated when the chemical environment of the photocatalyst is taken into account. For instance, it has been shown that the photocatalytic reactivity of TiO_2 strongly depends on the target substrate to probe [9]. Finally, although theoretical approaches can yield conceptual approaches to the design of specific properties [10–12], the design of operative complex configurations remains highly speculative. Hence, in

the absence of a generally acknowledged well-defined physical statement, systematic studies are required for in depth studies of the photo-catalytic phenomena. In this context, our recently reported production of dihydrogen (H₂) by daylight irradiation of TiO₂ supported Pt, has prompted the present work [13]. The H₂ generation has been performed with the simplest possible combination of sacrificial electron donor (ED), platinum supported TiO₂ nanoparticle (TiO₂/Pt) in aqueous solution (pH 6.5–7). Such a simple system allowed us to propose a specific mechanism based on radical generation at the nanoparticle/water interface. This step is the essential intermediate between the photon absorption and the subsequent catalytic reaction. This work extends the investigation of electron generation to three commercially available nano-TiO₂ with shared characteristics (e.g. density, energy gap or pH(PZC)) and differences (e.g. nanoparticle primary size, specific surface area or composition). The generation of electrons has been probed by Electronic Paramagnetic Resonance (EPR) spectroscopy using a spin scavenging like technique. At constant light intensity excitation and absorption condition, a systematic variation of the amount of TiO₂, the ED concentration and the pH, has been performed. Data on the optical behaviour and the aggregate state have been concomitantly collected. The obtained results are discussed along different routes based on the current knowledge without deciphering because of their interdependence.

Experimental

- Materials:

TiO₂ P25 was purchased from Degussa, TiO₂ AMT100 was purchased from Tayca and TiO₂ Hombicat UV100 was generous gift from Sachtleben Chemie. Ethylenediaminetetraacetic acid tetrasodium and disodium salts (EDTA) were purchased from Sigma Aldrich. 4-Hydroxy-2,2,6,6-tetramethylpiperidin-1-oxyl (TEMPOL) at 98% purity was purchased from Sigma–Aldrich. All these reagents were used as received. MilliQ water ($\rho = 18.2 \text{ M}\Omega \text{ cm}^{-1}$) was provided by a Millipore purification system.

- Measurements:

- Continuous-wave EPR X-band spectrometer (EMXplus from Bruker Biospin GmbH, Germany) was equipped with a high sensitivity resonator (4119HS-W1, Bruker). This setup was used to record the conventional field-swept spectra from the aqueous solutions containing photosensitizing solution together with TEMPOL molecules. EPR measurements were

performed in short intervals between the subsequent irradiation periods of 30 s. Prior to measurements, the final solutions (1 mL) were sonicated (15 min in a bath) and then deoxygenated by argon gas bubbling for at least 10 min. Afterwards, the solutions were immediately transferred into the thin-wall glass capillaries (Hirschmann rincaps, 20 μ L) and sealed on both ends. Illumination of the sealed aliquots was performed outside the cavity with a UV light source ($\lambda = 365$ nm i.e. $h\nu \cong 3.4$ eV and $E \cong 1.5$ mW cm^{-2} measured with a power meter 1936-C Newport). As TEMPOL does not absorb at this wavelength, there is no absorption variation during measurement [14]. The principal experimental parameters values were: modulation amplitude 0.5 G, microwave power 1.8 mW, time constant of ca. 20 ms, and 50 ms conversion time and 120 G were swept in 60 s per scan and 3 scans were accumulated. All experiments were performed at room temperature ($295 \text{ K} \pm 1 \text{ K}$).

- Dynamic Light Scattering (DLS) measurements were performed with a Malvern zetasizer nanoseries and a folded capillary cell. The data correspond to the number distribution. In order to start with mixed suspension, a sonication step (2 min) was performed prior measurement.

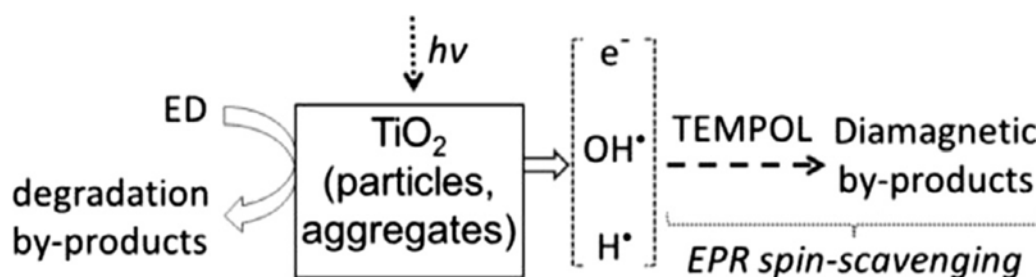
- UV-Vis measurements were performed with a Cary series UV-Vis-NIR 5000 spectrophotometer and a 1 cm path length cell. In order to start with mixed suspension, a sonication step (2 min in a bath) was performed prior measurement.

Results

The method implemented in this work can be compared to the one proposed in reported electron transfer processes in homogeneous systems [15]. The experimental approach used in our recent work [13] has been adapted to heterogeneous configuration to study the radical generation as sketched hereafter (Scheme 1).

As in the case of homogeneous conditions, an efficient electron donor (ED), EDTA, is required to limit parasitic electronic transfers that are involved in electron/hole recombination processes within the semiconductor bands. This approach is conceptually analogous to the photodegradation of pollutants. However, the main difference lies in the object that is probed in the study, namely the photogenerated entities instead of the degradation products of EDTA [16]. In the present anoxic experimental conditions, the photogenerated electrons in the conduction band is carried in solution by OH^\bullet and H^\bullet on the one side and by the spin scavenger via its direct reduction on the other side [2,17,18]. The presence of EDTA as efficient electron

donor precludes the oxidation process involving the spin scavenger [11]. Hence, TEMPOL probe has been chosen here because the steric hindrance induced by the presence of methyl groups around the nitroxide probe makes it more sensitive to small radical species [19]. Following this approach, all the electrons generated are taken into account. In this study, the nature (related to specific criteria mentioned below) and the amount of TiO₂ as well as the pH and the amount of electron donor have been varied in order to build a set of data rather than a case study to support our conclusions. In order to complete the radical photogeneration investigation, additional analyses have been performed to provide an exhaustive characterisation of the TiO₂ samples (elemental analysis, optical properties, aggregate size).



Scheme 1. Scheme of the concept used in this work for the electron generation measurements.

- Characterisation

Whereas numerous reported works have dealt with the various nano-TiO₂ used in this study, it felt relevant to obtain significant insights about their atomic composition. Although structural parameters, the specific surface area and the primary particles size (usually provided by the supplier) are commonly specified, the relative purity of the semiconductor is, in general, scarcely described. Table 1 presents a non-exhaustive elemental analysis for the three TiO₂ nanostructured materials.

The main information provided by the analysis is that the different TiO₂ do not contain the same amount of titanium. In the case of pure titanium oxide, the weight ratio of titanium is 59.9%. In the case of P25, the experimental value agrees with the expected one and corresponds to ca. 99% of titanium oxide. In the case of UV100 and AMT100, the experimental values yield a content of titanium oxide equal to ca. 90%, thus implying the presence of other components. Even though the analysis is not detailed, the information displayed in Table 1 shows that elements such as sodium, calcium or phosphorus are present in significant amount.

They can be subsequently considered as potential dopants, poisons or electron traps well-known to influence the photo-physical properties.

Element	TiO ₂		
	P25	UV100	AMT100
Ti (% w/w)	59 ± 2	53 ± 2	53 ± 1
Na (mg kg ⁻¹)	27 ± 4	1017 ± 15	319 ± 3
Mg (mg kg ⁻¹)	/	/	137 ± 2
Al (mg kg ⁻¹)	<2	2.6 ± 0.2	5.7 ± 0.1
Si (mg kg ⁻¹)	<30	<30	82 ± 3
P (mg kg ⁻¹)	<150	1930 ± 32	/
Ca (mg kg ⁻¹)	/	/	674 ± 12
Fe (mg kg ⁻¹)	<2	<2	30.7 ± 0.5

Table 1. Elemental analysis of the different nano-TiO₂ discussed in this study.

The data collected in Table 1 are intrinsic to each type of TiO₂ but other properties, particularly optical, are not intrinsic. As pointed out in the introduction, the object of this study is the semiconductor together within its environment (i.e. the suspension of the semiconductor in the presence of the electron donor). Fig. 1 shows the attenuation spectra obtained in aqueous suspension. Drastic differences exist between the three nano-TiO₂ systems, especially in the wavelength range where the light is absorbed (i.e. $\lambda < 400$ nm).

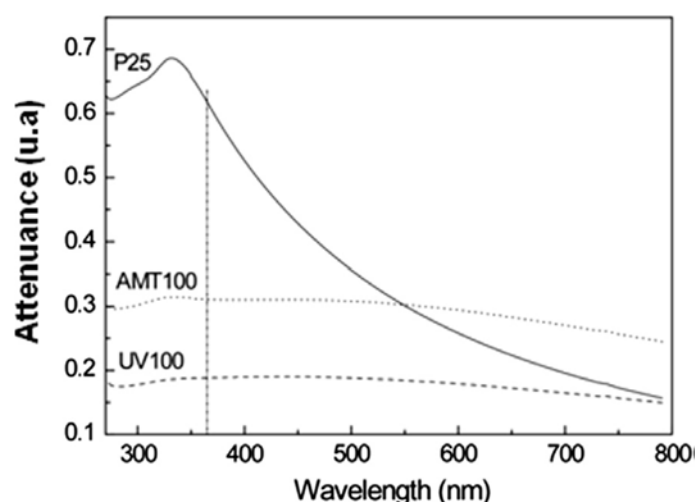


Fig. 1. UV-Vis attenuation spectra of nano-TiO₂ suspensions (0.025 g L⁻¹) in 0.025 M EDTA (pH = 6.5): P25 (solid line), AMT100 (dotted line) and UV100 (dashed line). The vertical dotted line shows the excited wavelength ($\lambda = 365$ nm) for the radical generation.

The contribution of the light diffusion is significantly larger for both semiconductor oxides having smaller primary size (UV100 and AMT100). The interpretation of this data is complex and requires careful investigations. In the context of well-dispersed systems, the Mie theory [20] usually provides general trends that take into account parameters such as the shape and morphology of particles interface possibly influencing the optical properties [21]. However, in this case, the aggregation phenomenon renders the situation more complex.

Typically, this complication is emphasized by DLS measurements performed (Fig. 2) on the different nano-TiO₂ aqueous suspensions. Remarkably, the results show similar value of hydrodynamic radii or diameters for the three kinds of titanium oxides aggregates. Because the hydrodynamic diameter does not correspond to the exact value of the aggregate dimension, precautions are necessary to extract relevant information. Noteworthy, recent reports have considered the fractal dimension in the context of TiO₂ aggregates [22,23].

Fractal dimension provides information about the shape and density of aggregates. These parameters are likely to influence the optical behaviour and the corresponding photochemical activity as well. Unfortunately, aggregation remains a limitation to probe the materials properties, although related to the characteristic of the nanoparticles [33]. Thus, the properties of the aggregates related to their specific environment and the nanoparticle elementary composition, encompass the intrinsic behaviour of individual nanoparticles by levelling down the expected optimal photoactivity.

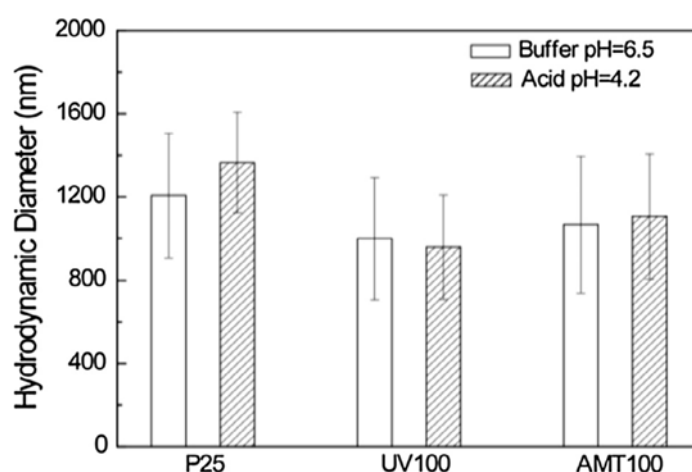


Fig. 2. Hydrodynamic diameter for the different sources of nano-TiO₂ (0.1 g L⁻¹), with EDTA (0.1 M) in buffering condition (pH = 6.5) and in acidic conditions (pH = 4.2). For each set of data, 6 samples were measured and provided 6 Gaussian distributions. A total distribution was built by summation of the 6 distributions. The presented data correspond to the maxima and the standard deviation (σ) of the total distribution. Noteworthy, neither the presence of TEMPOL (200 μ M) nor the time range (24 h) did not show any effect on the obtained value.

In [Table 2](#), comparative data for the three types of nano-TiO₂ is collected. As indicated above, the three nano-TiO₂ have been selected on a specific criteria: pH(PZC). Whatever is the nano-TiO₂, two acid/base equilibria, involving the surface functions Ti–OH, occur so that the pH(PZC) corresponds to 1/2(pK1 + pK2). Therefore, fixing the pH around the pH(PZC) should allow to impose Ti–OH as the predominant group. Moreover, despite the presence of elements other than titanium, the energy band gaps are similar for both UV100 and AMT100. Worthy of note, if small band gap variations have been observed depending of the nano-TiO₂ [34], the present light excitation energy (3.4 eV vs. 3.2 eV for bulk TiO₂ anatase) can overcome this requirement. Concerning the surface area parameter, a ratio larger than 5.5 is given between the UV100 or AMT100 when compared to P25. Additionally, the Ti–OH group densities Γ (mol cm⁻²) are comparable between UV100 and P25 [9].

TiO ₂	Structural composition ^a (%)		TiO ₂ (%)	Nanoparticle primary size diameter ^a (nm)	Density ^a (g cm ⁻³)	Surface area ^a (m ² g ⁻¹)	E_{gap} (eV)	pH in solution ^a	pH (PZC)
	A	R							
P25	≈80	≈20	≈99	21	3.8	≈50	3.0–3.2 ^{g,h,j}	3.5–4.5	6.4 ^c 6.3 ^e 6.9 ^d
AMT100	100	0	≈90	6	/	≈280	/	Neutral	/
UV100	100	0	≈90	10	3.9	≥300	3.1–3.2 ^{i,k,l}	Neutral	6.2 ^d 6.0 ^e

A: Anatase, R: Rutile, PZC: Point of Zero Charge, ^a obtained from the respective providers, ^b measured in this study, ^c from Ref. [24], ^d from Ref. [25], ^e from [9], ^f from Ref. [26], ^g from Ref. [27], ^h from Ref. [28], ⁱ from Ref. [29], ^j from Ref. [30], ^k from Ref. [31], ^l from Ref. [32]. (Although there is no value for AMT100, in view of the similarities of properties with UV100, it is reasonable to assume a comparable value of pH(PZC)).

Table 2. Characteristics of the nano-TiO₂ investigated in this work.

- EPR spin-scavenging

In our experimental approach ([Scheme 1](#)) in addition to the nature of the TiO₂, other parameters such as the amount of semiconductor, the amount of electron donor and the pH can be varied independently from each other. The experimental data are presented as the relative decay of the EPR intensity (I/I_0) related to the TEMPOL paramagnetic probe when reacting directly with electron from the conduction band and/or free radicals, leading to diamagnetic by-products (i.e. EPR silent). Hence, the I/I_0 decay is directly related to the rate of generation of photogenerated electrons. [Fig. 3](#) shows the data collected when the amount of oxide is changed by one order of magnitude (0.1 and 0.01 g L⁻¹).

Firstly, it can be noted that for the three different TiO₂, the results obtained are quite similar and, thus, do not reflect the surface area ratio (see [Table 2](#)). Secondly, the change of oxide amount can be clearly observed. The decay of the TEMPOL concentration (T^*) upon reaction with the photogenerated electrons can be modelled considering (i) the generation of radicals ($R^* = OH^*$ and H^*) and (ii) the direct reduction of the spin probe.

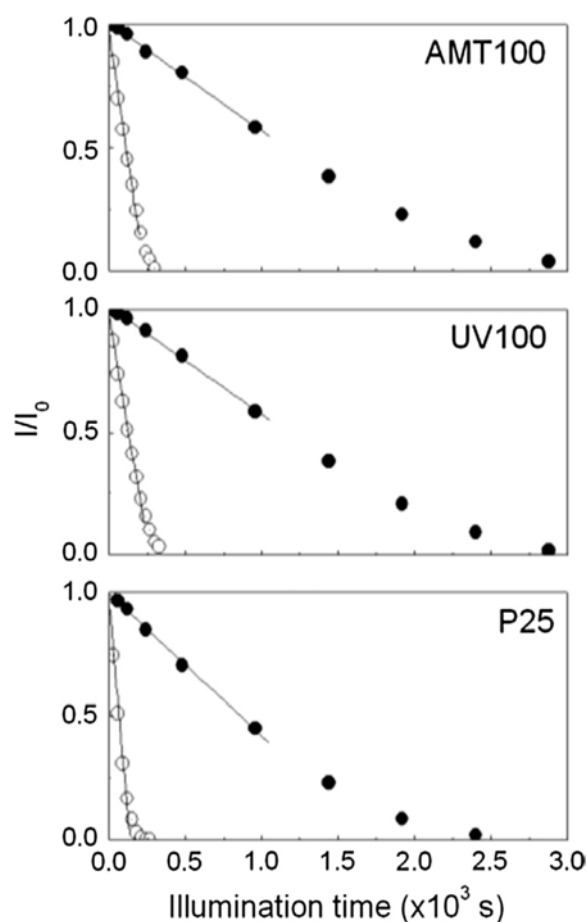


Fig. 3. TEMPOL normalized EPR intensities (I/I_0) as a function of illumination time (t) for 0.1 g L^{-1} (open circles) and 0.01 g L^{-1} (filled circles) of different nano-TiO₂: P25 (bottom), UV100 (central) and AMT100 (top). At $t = 0$ the concentration of TEMPOL and EDTA buffer ($\text{pH} = 6.5$) was $200 \text{ } \mu\text{M}$ and 0.1 M respectively. UV illumination intensity was ca. 1.5 mW cm^{-2} at $\lambda = 365 \text{ nm}$. A linear fit (solid line) was applied to all curves to determine the initial decay.

- Indirect reduction of TEMPOL with radicals

Radical generation involves electron transfer to surface groups such as $-\text{H}$ or $-\text{OH}$ which leave the interface after formation and react with TEMPOL. An equilibrium exists between TiO₂ surface groups and water via H^+ and OH^- exchanges. This involves that the amount of adsorbed species is constant with time. Thus, the photogenerated radicals H^\bullet and OH^\bullet either react with TEMPOL or form by-products very quickly (because of their short life time).

Then $\text{T}^\bullet + \text{R}^\bullet = \text{TR}$ display high kinetic constants. Under constant light illumination, there is no radical accumulation and the amount of radicals generated is low. The variation $d\text{R}^\bullet(t)/dt$ is close to zero (quasi steady state approximation), therefore $\text{R}^\bullet(t)$ is considered as constant.

Hence if Γ is the amount of adsorbed species (mol cm^{-2}), and A the area of TiO₂ (cm^2):

$$R^*(t) = k_1 A \Gamma' = k_1 (am)(b\Gamma) = mK_1\Gamma \text{ with } K_1 = abk_1 \quad (1)$$

given $A = am$ (m being the mass of TiO_2) and $\Gamma' = b\Gamma$ (the amount of radical is proportional to Γ).

For the reaction $T^* + R^* = TR$

$$- dT^*(t)/dt = k_2 R^*(t) T^*(t) = m\Gamma k_2 K_1 T^*(t) \quad (2)$$

$$dT^*(t)/T^*(t) = - m\Gamma K_2 dt \quad (3)$$

with the initial condition: $T^*(t=0) = T^*(0)$

$$T^*(t) = T^*(0) \exp(-m\Gamma K_2 t) \quad (4)$$

$$T^*(t)/T^*(0) = \exp(-m\Gamma K_2 t) \quad (5)$$

$$\text{And for short live time } T^*(t)/T^*(0) = 1 - m\Gamma K_2 t \quad (6)$$

- *Direct reduction of TEMPOL with TiO_2*

TEMPOL displays redox properties [17,18]

$T^* + e^- = T$ (redox potential = E_0)

The system EDTA/aggregate is equivalent to an electrode behavior and if collecting the electrons (i.e. measuring the current) under light illumination of the suspension, corresponds to build a potential step ($\Delta E = E_{gap}$). This phenomenon is equivalent to a bulk electrolysis, assuming fast electrode transfer kinetic.

If the potential is in the limiting current region i.e. where diffusion mass transport is the limiting process ($E \gg E_0$), we have [35]:

$$I(t) = nFAM T^*(t) \quad (7)$$

where n is the number of exchanged electrons, F is the faraday constant, A ($A = am$) the surface of the electrode and M is in cm s^{-1} . The current $I(t)$ (C s^{-1}) corresponds to the number of electrons $N_{T\cdot}$ transferred per time unit due to the reduction of the TEMPOL (mol s^{-1}).

$$I(t) = -nF \frac{dN_{T\cdot}(t)}{dt} = -nFV \frac{dT^*(t)}{dt} \quad (8)$$

with V being the volume of solution, hence:

$$-nFV \frac{dT^*(t)}{dt} = nFAM T^*(t) \quad (9)$$

$$\frac{dT^*(t)}{dt} = -(AM/V) T^*(t) \quad (10)$$

with the initial condition $T^*(t = 0) = T^*(0)$

$$T^*(t) = T^*(0) \exp(-(AM/V)t) = T^*(0) \exp(-mK_3t) \quad (11)$$

$$T^*(t)/T^*(0) = \exp(-mK_3t) \quad (12)$$

$$\text{And for short time we obtain } T^*(t)/T^*(0) = 1 - mK_3t \quad (13)$$

- *Combination of the two reduction pathways*

Considering that both processes contribute to the decay of the TEMPOL concentration:

$$T^*(t)/T^*(0) = \alpha \exp(-m\Gamma K_2t) + \beta \exp(-mK_3t) \text{ with } \alpha + \beta = 1 \quad (14)$$

For short time

$$\begin{aligned} T^*(t)/T^*(0) &= \alpha(1 - m\Gamma K_2t) + \beta(1 - mK_3t) \\ &= (\alpha + \beta) - m(\alpha\Gamma K_2 + \beta K_3)t \\ &= 1 - m(\alpha\Gamma K_2 + \beta K_3)t \end{aligned} \quad (15)$$

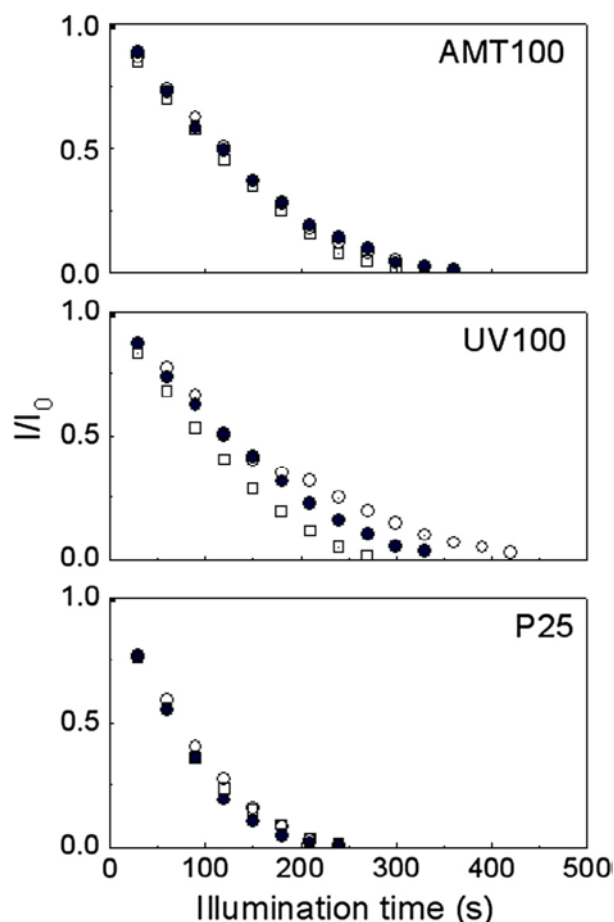


Fig. 4. TEMPOL normalized EPR intensities (I/I_0) as a function of illumination time (t) for different nano-TiO₂ (at 0.1 g L^{-1}): P25 (bottom), UV100 (central) and AMT100 (top). EDTA was used in buffering condition ($\text{pH} = 6.5$) at 0.1 M (closed circle) and 0.01 M (open circle) and in acidic conditions ($\text{pH} = 4.2$) at 0.1 M (open square). UV illumination intensity was ca. 1.5 mW cm^{-2} at $\lambda = 365 \text{ nm}$. At $t = 0$ the concentration of TEMPOL was $200 \text{ }\mu\text{M}$.

As the EPR intensity I is proportional to $[T^*]$: $I = qT^*$, the data in Fig. 3 are consistent with this model. Focusing on short time, relative slopes have been assessed. When the amount of oxide is 0.1 g L^{-1} , the values obtained are -7×10^{-3} (P25), -4×10^{-3} (UV100), -4×10^{-3} (AMT100) and -6×10^{-4} (P25), -4×10^{-4} (UV100), -4×10^{-4} (AMT100) for 0.01 g L^{-1} of nano-TiO₂. Considering that all parameters are kept unchanged, these data indicate a major trend: the generation of electrons depends linearly on the mass of oxide. Nevertheless, this conclusion is only valid in the context where no other step of the process can be considered as a limiting factor. In order to investigate the electron donation process, measurements have been performed with a concentration of EDTA ten times lower i.e. 0.01 M . The corresponding results presented in Fig.

4 indicate no significant changes, which suggest that the generation of electrons is similar in this range of EDTA concentration (0.1–0.01 M). Thus, a limiting step involving the electron donation process can be excluded. Evidence for the efficiency of EDTA as an electron donor is deduced from the linear dependence of the generation of electrons from amount of nano-TiO₂ (Fig. 3). Therefore, in the present situation the light absorption linearly depends on the amount of the active species (i.e. like for the Beer–Lambert law for light absorbance of homogenous molecules in solution). It is thus considered that the current experimental conditions allow the collection of well-defined and quantitative data for the photogenerated electrons and it is now possible to focus on the comparison of each TiO₂ samples. As already mentioned and confirmed by the slope values, the generation of electrons appears remarkably analogous. A slightly higher rate for P25 can be pointed out. This is again surprising when the specific characteristics of each TiO₂ are taken into account.

Discussion

It is essential to consider the experimental conditions as a complex combination of interdependent parameters, which are difficult to investigate separately. A synergetic effect rutile/anatase could be involved for P25 but several parameters that may be responsible for the levelling of the obtained results will be discussed hereafter.

Typically, the photon absorption is the first variable. As observed in Fig. 1, the transmission measurements show a strikingly different behaviour for the three nano-TiO₂ batches. On the one hand, this type of result cannot be considered as significant regarding the absorption properties but it points at discrepancies in the optical properties. These variations are related to the primary size, the particles morphology and the aggregation state through the Mie (and Rayleigh) theory [20]. On the other hand, varying the aggregation state while keeping an identical aqueous environment appears difficult without affecting the nature of the aggregate itself. Consequently, it seems difficult to untangle these parameters and probe their influence separately. Ideally, one option would be to obtain monodispersed nano-TiO₂, which seems very challenging without adding specific agents and affecting the direct environment of the particle [36]. Another approach could involve a careful nano-structuration of surfaces, to fix the parameters that are not controlled in suspension. Additionally, the intensity of the absorbed light remains an important factor and the effects of an increase in the specific

surface area while keeping a relatively low light intensity can be questioned. In the perspective of applicative device, an increase of the power of incident irradiation would be of less concern than the effort made to operate in realistic conditions. Therefore, our irradiation conditions (ca. 1.5mWcm⁻² at $\lambda = 365$ nm) have been defined in agreement with the UV part of the solar spectrum (ca. 4–5mWcm⁻² in the AM 1.5 spectrum) [37]. Moreover, the quantum yield of nano-TiO₂ being usually low [1,38], the potential performances expected for each oxide are far to be reached: no matter is the surface area, it is not obvious that this parameter comes in play. The independence of EDTA concentration in the range 0.01–0.1 M for the electron generation (Fig. 4) can be seen as indicative of this possible effect. A third variable involves the density and shape of aggregates through the fractal dimension (see results section) [22,23]. Whereas in gas phase, aggregation can only have a small impact [39], the latter may be larger in solution. Whatever are the processes (catalysis, photoluminescence or spin scavenging), the common step is the encounter between species produced in the vicinity of the interface between the solid phase and the reactant in solution. Either the reaction takes place at the solid/liquid interface itself or in solution: in order to compare directly different nano-TiO₂ the number of particles has to be similar as well as the accessibility of their interface. These requirements are not easily fulfilled when dealing with oxides displaying discrepancies in the shape and density of their aggregates. A parallel can be drawn at the scale of the nanoparticles in solution about the relevance of the specific surface area through the accessibility of the pores. Given a similar density (see Table 2), smooth particles and a similar size of aggregates in solution (Fig. 2) we have:

The number of particles in one aggregate is V/V_p .

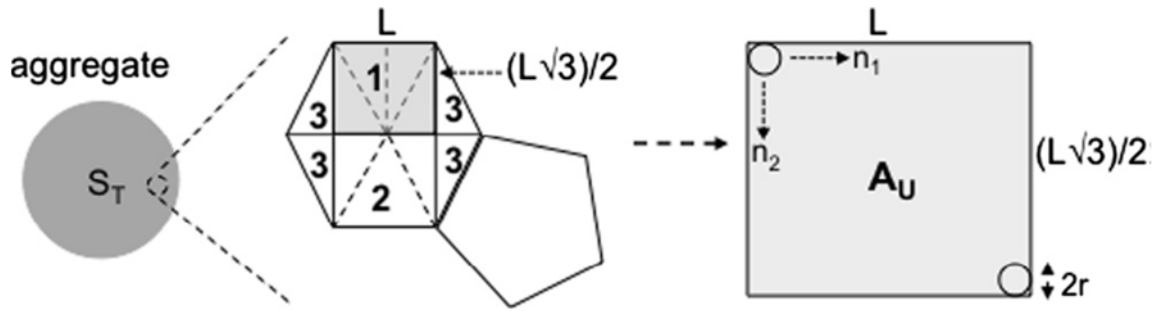
And the number of particles in 1 g is $V_{1g}/V_p = 1/d \cdot V_p$, where V is the volume of one aggregate, V_p the volume of one particle, d the real density (g cm⁻³) and $V_{1g} = 1/d$, the volume of 1 g of TiO₂. The number of aggregates in solution (N_{aq}) is then

$$[1/(d \cdot V_p)] / (V/V_p) = 1/(d \cdot V) \quad (16)$$

Hence, in this basic model N_{aq} is independent of V_p i.e. for the same density and mass of material in solution, the number of aggregates is the same whatever the particles size.

For the reason explained above, only the radicals and electrons generated by the surrounding area of the aggregates are expected to mainly react with the molecules from the bulk solution.

In other words, the participation of the inner part of the aggregates can be considered as negligible. In such approach, the external surface (S_T) of the aggregates is evaluated in the context of hard sphere model and an ideally null porosity of the particles. Paving a sphere with hexagons and pentagons, a unit cell of surface A_U is available (Scheme 2).



Scheme 2. Definition of a unit surface cell when paving a spherical aggregate having an external surface S_T .

Considering the surface of one hexagon (A_H):

$$A_H = (3L^2\sqrt{3})/2 = 3L(L\sqrt{3})/2 = 3A_U \quad (17)$$

Hence, the number of particles (of radius r) in a row (n_1) is: $L/2r$ whereas the number of particles in a column (n_2) is: $(L\sqrt{3})/4r$. Thus, the total number of particles in the unit cell $n^2 = n_1n_2 = (L^2\sqrt{3})/8r^2$. For each particle, the same ratio of available surface (S_P) is assumed: $S_P = (4\pi r^2)/m$, with $m = 2$ in the case of an half sphere for instance. Therefore, the Total surface in the Unit cell is

$$A_{TU} = n^2S_P = (\pi L^2\sqrt{3})/2m \quad (18)$$

Considering the surface of one pentagon (A_P), for regular polygons with b sides ($b > 3$), the area A is:

$$A = bL^2/\tan(\pi/b) \quad (19)$$

And

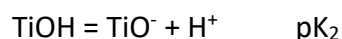
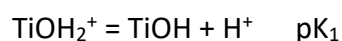
$$A_P/A_H = Cst = [6\tan(\pi/6)]/[5\tan(\pi/5)] = K \quad (20)$$

Thus, the total external surface (ST) of the aggregate is (for x hexagons and 12 pentagons):

$$S_T = xA_H + 12 A_P = xA_H + 12KA_H = 3(x+12K) A_{TU} \quad (21)$$

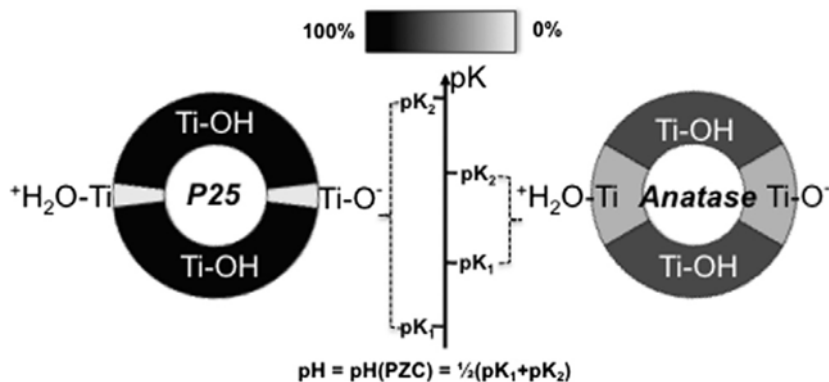
In this hypothesis, both the number of aggregates and the total external surface are independent of the particle size and thus, the active surface is equivalent whatever is the nano-TiO₂ source. As mentioned above, P25 and UV100 display similar Γ values. Thus, when considering the proposed model for the TEMPOL decay (indirect and direct reduction), equivalent active surfaces are assumed to interpret the results. Even though these considerations are idealistic, it supports the hypothesis of the low influence in solution of the specific surface area.

The last experimental parameter discussed hereafter is the pH. TiO₂ has two acid/base equilibriums:



Examples of pH influence are found for the oxide energy bands [1], the photoactivity or the nature of the generated radicals [40]. Associated to this notion, the pH(PZC) is often considered because of its indication of the zero charge. From data in Table 2, P25 and UV100 materials present comparable pH(PZC) value. Fig. 4 displays the electron detection at pH = 4.2 and 6.5 for the three types of TiO₂. If no significant differences are observable, the hydrogen generation changes with the pH in the case of P25 nano-TiO₂ [13]. In anaerobic conditions only OH[•] and H[•] are expected and a recent study pointed out a higher generation of OH[•] at lower pH [40]. On the one side, because EDTA exhibits particular adsorption [41], the possibility of direct or indirect electron transfer, involving hydroxyl radicals, related to the pH dependent variation of the adsorption processes has to be considered [42]. On the other side, the distribution of the nature of the surface groups is function of the nano-TiO₂ origin and thus the pH has to be scrutinized carefully for comparative studies. If the pH(PZC) is consistent with

$1/2(pK_1 + pK_2)$, several couples of pK can provide the same pH (PZC) but leading to different ratio of protonated/unprotonated surface functions at same pH (see [Scheme 3](#)).



Scheme 3. Ideal relative proportion of the protonated–neutral-unprotonated surface groups, for $pH = pH(PZC)$, as a function of nano-TiO₂ origin: P25 (4–92–4% respectively) and Anatase (16.5–67–16.5% respectively).

It is indeed the case for P25 and anatase particles as reported in the work of Ohtani et al. [24]. Assuming identical properties for all the Ti–OH functions, for $pH = pH(PZC)$, P25 is in the configuration of $(pK_1 + 1.4)$ and $(pK_2 - 1.4)$ whereas for anatase, we have $(pK_1 + 0.6)$ and $(pK_2 - 0.6)$. Consequently, almost 100% of surface groups are of Ti–OH type in the case of P25 vs. only 67% (16.5% TiOH₂⁺ and 16.5% TiO⁻) in the case of anatase, as shown in [Scheme 3](#). Such differences can have a significant impact on the possible mechanisms of the surface reactivity [43,44].

Conclusion

This study focused on the comparison of photogenerated electrons by different commercially available nano-TiO₂ (P25, UV100 and AMT100). The investigation involved a model system implying ED (electron donor)/TiO₂/detection, i.e. free of additional step such as catalysis. Despite environmental conditions as comparable as possible, equivalent apparent parameters (energy gap, pH(PZC) and hydrodynamic diameter) and deliberately different (primary particle size, specific surface area or composition), the results showed similar behaviour, apparently independent to the relevant factors.

This study shows that the comparison and the interpretation of the intrinsic properties for several aqueous nano-TiO₂ are complicated by the use of suspensions. This is mostly due to the interdependence of the parameters influencing the apparent properties of the nanomaterials via equalizing effects.

Because the suspension configuration hinders and/or levels the potential properties of the different nano-materials, a comprehensive approach involving: light absorption properties, aggregate size, aggregate shape, aggregate density, pH investigation and the development of methods allowing to modulate only one parameter independently from the others would be necessary for each configuration nano-TiO₂/environment system.

We have pointed out the difficulties to understand the molecular mechanisms underlying the photocatalytic properties of nano-TiO₂ that are nevertheless required to improve the efficiency of applicative devices. The nanostructuring of surfaces [45] appears here as a better approach for the investigation of such fundamental questions, as the parameters discussed above can be monitored.

Acknowledgements

This study was supported by the Centre National de la Recherche Scientifique (CNRS) and Université de Strasbourg. We gratefully acknowledge Karima Boutellaa for her kind help in the EPR experiments. We thank the French Ministry of Research and the REseau NATional de Rpe interDisciplinaire (RENARD, Fédération IR-RPE CNRS #3443).

References

- [1] A. Fujishima, X. Zhang, D.A. Tryk, *Surf. Sci. Rep.* 63 **2008** 515–582.
- [2] A. Fujishima, K. Honda, *Nature* 238 **1972** 37–38.
- [3] H.M. Chen, C.K. Chen, R.-S. Liu, L. Zhang, J. Zhang, D.P. Wilkinson, *Chem. Soc. Rev.* 41 **2012** 5654–5971.
- [4] T. Yoshida, S. Niimi, M. Yamamoto, T. Nomoto, S. Yagi, *J. Coll. Inter. Sci.* 447 **2015** 278–281.
- [5] L. Li, B. Cheng, Y. Wang, J. Yu, *J. Coll. Inter. Sci.* 449 **2015** 115–121.
- [6] O. Solcova, T. Balkan, Z. Guler, M. Morozova, P. Dytrych, A.S. Sarac, *Sci. Adv. Mater.* 6 **2014** 2618–2624.
- [7] M.A. Henderson, *Surf. Sci. Rep.* 66 **2011** 185–297.

- [8] B. Ohtani, O.O. Prieto-Mahaney, D. Li, R. Abe, *Photochem. Photobiol. A: Chem.* 216 **2010** 179–182.
- [9] J. Ryu, W. Choi, *Environ. Sci. Technol.* 42 **2008** 294–300.
- [10] A.S. Bernard, P. Zapol, *Phys. Rev. B* 70 (235403) **2004** 1–13.
- [11] H. Lin, C.P. Huang, W. Li, C. Ni, S. Ismat Shah, Y.-H. Tseng, *Appl. Catal. B* 68 **2006** 1–11.
- [12] M. Ribeiro, S. Shevlin, *Sci. Adv. Mater.* 7 **2015** 623–630.
- [13] B. Vileno, P. Turek, J. Weiss, D. Martel, *ChemPlusChem* 78 **2013** 1330–1333.
- [14] A. Turolla, A. Piazzoli, J. Farner Budarz, M.R. Wiesner, M. Antonelli, *Chem. Eng. J.* 271 **2015** 260–268.
- [15] K. Kalyanasundaram, J. Kiwi, M. Grätzel, *Helv. Chim. Acta* 61 **1978** 2720–2730.
- [16] R.T. Belly, J.J. Lauff, C.T. Goodhue, *Appl. Microbiol.* 29 **1975** 787–794.
- [17] P. Bar-On, M. Mohsen, R. Zhang, E. Feigin, M. Chevion, A. Samuni, *J. Am. Chem. Soc.* 121 **1999** 8070–8073.
- [18] J.P. Blinco, J.L. Hodgson, B.J. Morrow, J.R. Walker, G.D. Will, M.L. Coote, S.E. Bottle, *J. Org. Chem.* 73 **2008** 6763–6771.
- [19] K. Matsumoto, K. Nagata, H. Yamamoto, K. Endo, K. Anzai, I. Aoki, *Magn. Reson. Med.* 61 **2009** 1033–1039.
- [20] J.W. Hovenier, M.I. Mishchenko, W.J. Wiscombe, L.D. Travis, Overview of scattering by nonspherical particles, in: M.I. Mishchenko, J.W. Hovenier, L.D. Travis (Eds.), *Light Scattering by Nonspherical Particles: Theory, Measurements, and Applications*, 2000.
- [21] B. Hapke, *J. Geophys. Res.* 86 **1981** 3039–3054.
- [22] D. Jassby, J. Farner Budarz, M. Wiesner, *Environ. Sci. Technol.* 46 **2012** 6934–6941.
- [23] I. Chowdhury, S.L. Walker, S.E. Mylon, *Environ. Sci.: Process Impacts* 15 **2013** 275–282.
- [24] B. Ohtani, Y. Okugawa, S. Nishimoto, T. Kagiya, *J. Phys. Chem.* 91 **1987** 3550–3555.
- [25] P.K. Dutta, A.K. Ray, V.K. Sharma, F.J. Millero, *J. Coll. Inter. Sci.* 278 **2004** 270–275.
- [26] R. Al-Rasheed, D.J. Cardin, *Appl. Catal. A* 246 **2003** 39–48.
- [27] M. Wojtoniszak, B. Zielinska, X. Chen, R.J. Kalenczuk, E. Borowiak-Palen, *J. Mater. Sci.* 47 **2012** 3185–3190.
- [28] F. Oshani, R. Marandi, S. Rasouli, M.K. Farhoud, *Appl. Surf. Sci.* 311 **2014** 308–313.
- [29] F. Pei, Y. Liu, S. Xu, J. Lü, C. Wang, S. Cao, *Int. J. Hydrogen Energy* 38 **2013** 2670–2677.
- [30] M.A. Behnajady, M.E. Alamdari, N. Modirshahla, *Environ. Prot. Eng.* 39 **2013** 33–46.
- [31] P.-W. Chou, S. Treschev, P.-H. Chung, C.-L. Cheng, Y.-H. Tseng, Y.-J. Chen, M.S. Wong, *Appl. Phys. Lett.* 89 **2006** 131919.
- [32] C.-H. Huang, Y.-M. Lin, I.-K. Wang, C.-M. Lu, *Int. J. Photoenergy* **2012** 548647.
- [33] T.A. Egerton, I.R. Tooley, *J. Phys. Chem. B* 108 **2004** 5066–5072.
- [34] V. Luca, *J. Phys. Chem. C* 113 **2009** 6367–6380.
- [35] A.J. Bard, L.R. Faulkner, *Electrochemical Methods: Fundamentals and Applications*, second ed., John Wiley & Sons Inc., 2001.
- [36] N. Veronovski, P. Andreozzi, C. La Mesa, M. Sfiligoj-Smole, *Surf. Coat. Technol.* 204 **2010** 1445–1451.
- [37] <http://rredc.nrel.gov/solar/spectra/am1.5/>.
- [38] K. Ishibashi, A. Fujishima, T. Watanabe, K. Hashimoto, *J. Photochem. Photobiol., A* 134 **2000** 139–142.
- [39] A.J. Maira, K.L. Yeung, C.Y. Lee, P.L. Yue, C.K. Chan, *J. Catal.* 192 **2000** 185–196.
- [40] Q.J. Xiang, J.G. Yu, P.K. Wong, *J. Coll. Inter. Sci.* 357 **2011** 163–167.
- [41] G. Kim, W. Choi, *Appl. Catal. B* 100 **2010** 77–83.

- [42] T.L. Villarreal, R. Gómez, M. Neumann-Spallart, N. Alonso-Vante, P. Salvador, *J. Phys. Chem. B* 108 **2004** 15172–15181.
- [43] N. Sakai, A. Fujishima, T. Watanabe, K. Hashimoto, *J. Phys. Chem. B* 107 **2003** 1028–1035.
- [44] R. Nakamura, Y. Nakato, *J. Am. Chem. Soc.* 126 **2004** 1290–1298.
- [45] P. Kondaiah, V. Madhavi, M. Chandra Sekhar, G. Mohan Rao, S. Uthanna, *Sci. Adv. Mater.* 7 **2015** 1640–1648.